Inverse cascade suppression and shear layer formation in MHD turbulence subject to a strong background magnetic field and misaligned global rotation

Santiago J. Benavides[1]†, Keaton J. Burns[2,3], Basile Gallet[4], James Y-K. Cho[3,5] and Glenn R. Flierl[1]

[1]Department of Earth, Atmospheric, and Planetary Sciences, Massachusetts Institute of Technology, Cambridge, MA 02139, USA

[2]Department of Mathematics, Massachusetts Institute of Technology, Cambridge, MA 02139, USA

[3]Center for Computational Astrophysics, Flatiron Institute, Simons Foundation, New York, NY 10010, USA

[4]Service de Physique de l'État Condensé, CEA, CNRS UMR 3680, Université Paris-Saclay, CEA Saclay, 91191 Gif-sur-Yvette, France

[5]School of Physics and Astronomy, Queen Mary University of London, Mile End Road, London E1 4NS, UK

(Received xx; revised xx; accepted xx)

Astrophysical plasmas are often subject to both rotation and large-scale background magnetic fields. Individually, each is known to two-dimensionalize the flow in the perpendicular plane. In realistic flows, both of these effects are simultaneously present and, importantly, need not be aligned. In this work, we numerically investigate three-dimensional forced magnetohydrodynamic (MHD) turbulence subject to the competing effects of global rotation and a background magnetic field, when the global rotation vector and the magnetic field are perpendicular. Focusing on the case of a strong background field and increasing the rotation rate from zero produces significant changes in the structure of the turbulent flow. Starting from a two-dimensional inverse cascade scenario at zero rotation, the flow transitions to a forward cascade of kinetic energy, then a shear-layer dominated regime, and finally a second shear-layer regime where the kinetic energy flux is strongly suppressed and the energy transfer is purely mediated by the induced magnetic field. We show that these transitions are sharp yet distinct in behavior, with one displaying hysteresis. Furthermore, we find more generally that, when considering the limit of strong rotation and strong magnetic field, the order in which those limits are taken matters.

1. Introduction

The behavior of three-dimensional (3D) turbulence in idealized settings beyond the homogeneous and isotropic case is not well understood (Frisch 1995; Alexakis & Biferale 2018). This includes, but is not limited to, rotating, ionized, stratified, and large aspect ratio systems, all of which are important characteristics of geophysical and astrophysical flows. Asymptotic regimes are sought out to simplify the system, often times restoring isotropy and thus allowing previous ideas and techniques of idealized turbulence to be

† Email address for correspondence: santib@mit.edu

used. This is done by studying the limiting equations as a control parameter (rotation, aspect ratio, etc.) is taken to zero or infinity. For example, one particular success is the quasigeostrophic approximation in rapidly rotating systems, which predicts two-dimensional (2D) flow in the plane perpendicular to rotation (Vallis 2017; Buzzicotti *et al.* 2018). A similar simplification occurs in plasmas in the presence of a strong uniform background magnetic field, reducing the dynamics to 2D magnetohydrodynamics (MHD) (Montgomery & Turner 1981), resulting in 2D hydrodynamics (HD) if the magnetic field isn't forced (Alexakis 2011). Both of these examples produce 2D HD turbulence, which is characterized by the presence of an *inverse cascade* of energy, in which energy goes from the forcing scale towards larger scales (Boffetta & Ecke 2012; Alexakis & Biferale 2018). This is in contrast to the forward energy cascades found in 3D HD and isotropic MHD turbulence, where energy cascades to smaller scales. The asymptotic regimes allow one to use energy cascade arguments for the understanding of turbulent geophysical and astrophysical phenomena. For example, the inverse cascade in the quasigeostrophic system is thought to be necessary for the formation of jets in rapidly rotating planetary atmospheres (Rhines 1975; Tobias *et al.* 2007). An analogous mechanism is thought to be responsible for the formation of poloidal jets in tokamak plasmas in the presence of a strong background toroidal 'guiding' magnetic field (Diamond *et al.* 2005).

In many geophysical and astrophysical contexts, however, it is expected that a fluid is subject to some combination of rotation, ionization, or stratification. Asymptotic analysis of these combined cases is more difficult, where often the order of the limits do not commute, and knowing which regime is observed in nature (and how the energy cascades behave) is a challenge [CITE]. Furthermore, real physical systems are not subject to infinite rotation rates or infinite background magnetic field strengths and reality often lies at intermediate values. There is currently no existing theory for the cascade direction of such intermediate parameters, and it is only more recently through state-of-the-art simulations that we are able to carefully investigate their turbulent dynamics. Numerical studies looking into the cascade of conserved quantities in these geophysical and astrophysical flows have revealed the presence of *bidirectional cascades*† at intermediate parameter values, in which a fraction of the conserved quantity input by the forcing goes to large scales whereas the rest goes to small scales (Alexakis & Biferale 2018; Pouquet *et al.* 2019). Most of these systems seem to form bidirectional cascades at particular *critical* values of the control parameters, revealing further unexpected complexity. Numerical tools are crucial in revealing the behavior of turbulent systems in configurations and parameter values that are out of reach of asymptotic methods.

Here we investigate the turbulent dynamics of an incompressible MHD fluid subject to rotation and a *misaligned* uniform background magnetic field using a series of direct numerical simulations. Such a configuration is expected to represent the turbulent dynamics in the atmospheres of gas giant planets, in the transition region between the outer, neutral atmosphere and the deep, ionized one (Benavides & Flierl 2020). There, the dynamics are characterized by rapid rotation and the presence of a strong background field generated by the dynamo in the deep interior region below. Given the prevalence of astrophysical systems which are both ionized and undergoing rotation, we expect our results to be general enough to apply in other contexts.

In particular, we're interested in understanding what happens when you have two, two-dimensionalizing effects which act in different directions. What is the fate of the inverse

† Not to be confused with *dual* cascade scenarios, where the system has two conserved quadratic conserved quantities which cascade in different directions, such as in 2D HD turbulence with the forward cascade of enstrophy and inverse cascade of energy.

cascade and how 'fragile' is it to variation in the secondary control parameter? Focusing on the case of a strong background field, we find that increasing the rotation rate from zero produces significant changes in the structure of the turbulent flow. Starting from a two-dimensional inverse cascade scenario at zero rotation, we find four distinct dynamical regimes: for weak rotation rate we observe a bidirectional cascade of kinetic energy, with energy flux to large scales decreasing as rotation is increased, and negligible induced magnetic energy. For rotation rates past some critical point, the flow transitions to a purely forward cascade of kinetic energy. Further increasing the rotation rate results in a shear-layer dominated regime, where nonlinearities at large scales are suppressed. Finally, at the largest rotation rates we investigated, we found a second shear-layer regime where the induced magnetic energy is no longer negligible, the kinetic energy flux is strongly suppressed and the energy transfer is purely mediated by the induced magnetic field. Using a two-dimensional, three-component asymptotic model of our system, we also show that the first three regimes are separated by sharp transitions, hinting at the existence of a bifurcation in the behavior of the nonlinear terms. One is found to be similar to other previously-found transitions from a bidrectional cascade to a forward one, while the other shows subcritical behavior including a discontinuity in the order parameter and hysteresis. The transition to the magnetically active regime is less understood, but we show that it also sharpens towards a critical value as the background magnetic field strength increases. We find more generally that, when considering the limit of strong rotation and strong magnetic field, the order in which those limits are taken matters.

In section 2 we introduce the system we will study: rotating MHD in the presence of a background magnetic field (RMHDB), also referred to as $B\Omega$-MHD (Menu *et al.* 2019). In section 3 we discuss results from three-dimensional simulations in which the background magnetic field is strong and as we vary the rotation rate in a perpendicular direction. In section 4 we introduce an asymptotic model (similar to that derived in Montgomery & Turner (1981)) representing the strong background magnetic field limit and including rotation, and discuss results from the two-dimensional three-component (2D3C) simulations of that system. Discussion and implications of our results are presented in section 5.

2. Rotating MHD in the presence of a background magnetic field

The equations for rotating magnetohydrodynamics in the presence of a uniform background magnetic field are (Shebalin 2006; Galtier 2014):

$$\frac{\partial \boldsymbol{v}}{\partial t} + (\boldsymbol{v}\cdot\nabla)\boldsymbol{v} = -\frac{1}{\rho_0}\nabla p^* - 2\boldsymbol{\Omega}\times\boldsymbol{v} + \frac{1}{\rho_0}\boldsymbol{j}\times(\boldsymbol{B_0}+\boldsymbol{b}) + \nu\nabla^2\boldsymbol{v} + \boldsymbol{f}, \tag{2.1}$$

$$\frac{\partial \boldsymbol{b}}{\partial t} + (\boldsymbol{v}\cdot\nabla)\boldsymbol{b} = (\boldsymbol{B_0}\cdot\nabla)\boldsymbol{v} + (\boldsymbol{b}\cdot\nabla)\boldsymbol{v} + \eta\nabla^2\boldsymbol{b}, \tag{2.2}$$

$$\boldsymbol{j} = \frac{1}{\mu_0}\nabla\times\boldsymbol{b}, \quad \nabla\cdot\boldsymbol{v} = 0, \quad \nabla\cdot\boldsymbol{b} = 0, \tag{2.3}$$

where $\boldsymbol{v} = (v_x, v_y, v_z)$ is the velocity field and $\boldsymbol{b}$ is the induced magnetic field, making up the two dynamical variables in this system. The two control parameters are $\boldsymbol{\Omega}$, the global rotation vector (with magnitude Ω), and $\boldsymbol{B_0}$, the uniform background field (with magnitude B_0). Other definitions include the current $\boldsymbol{j}$, the total pressure modified by rotation p^*, the constant density ρ_0, and the diffusion terms: ν is the kinematic viscosity, and $\eta = (\mu_0\sigma)^{-1}$ is the magnetic diffusivity, where σ is the conductivity and μ_0 is the magnetic permeability. Finally, $\boldsymbol{f}$ is a body force, which will be used to inject energy into the velocity field.

The inviscid and perfectly conducting system conserves only the total energy,

$$E = \frac{1}{2}\int \left(\boldsymbol{v}^2 + \frac{\boldsymbol{b}^2}{\rho_0\mu_0} \right) \, d^3x. \tag{2.4}$$

However, when $\boldsymbol{\Omega}$ and $\boldsymbol{B_0}$ are collinear, this system also conserves what's known as the *parallel*-(Shebalin 2006) or *hybrid-helicity* (Galtier 2014; Menu *et al.* 2019). The collinear system has gotten considerable attention – favored over the misaligned case in part due to its extra conserved quantity and the potential relevance of its cascade for dynamo action(Shebalin 2006; Menu *et al.* 2019). It also possesses simplified linear wave solutions, taken into consideration in the development of a weak wave turbulence theory (Galtier 2014; Bell & Nazarenko 2019). Here we will *not* be considering the collinear case, and so only the total energy will be conserved in our study of RMHDB in section 3. Although waves are certainly present in our system, our work concerns the strongly turbulent dynamics of energy cascades (present partly in the zero frequency modes of the system).

Most studies, with rotation and background magnetic field aligned or not, have focused on how rotation and a moderate background field affect the decay of kinetic and magnetic energies in unforced simulations (Lehnert 1955; Favier *et al.* 2012; Bell & Nazarenko 2019; Baklouti *et al.* 2019). Menu *et al.* (2019) investigated the sensitivity of the cascade of hybrid helicity for various alignments in forced-dissipative simulations. We are the first to consider the effects of rotation and a misaligned background magnetic field on the two-dimensionalization of the flow and the energy cascade, including the limits of strong rotation and strong background magnetic field.

In our study, the rotation and background magnetic field vectors are perpendicular to each other, namely, we've chosen $\boldsymbol{\Omega} = \Omega\hat{\boldsymbol{z}}$ and $\boldsymbol{B_0} = B_0\hat{\boldsymbol{x}}$. The strength of the background field is measured by a dimensionless number comparing the Alfvén wave speed to a typical velocity U:

$$V_A \equiv \frac{B_0}{\sqrt{\mu_0\rho_0}\, U}. \tag{2.5}$$

This dimensionless number can also be thought of as a measure of how the third term on the right hand side of equation (2.1) (the Lorentz force) and the first term on the right hand side of equation (2.2) compare to the advection terms in each respective equation, which would determine whether or not the background field affects the dominant dynamics. When $V_A \gg 1$ the Lorentz force acts to constrain the velocity and induced magnetic fields so that they don't vary along the x-direction, e.g. most of the energy lies in the $k_x = 0$ modes, resulting in 2D MHD (Montgomery & Turner 1981) occurring in the y-z plane. If the induced magnetic field isn't directly forced (as is the case in our study), it has been observed to decay, resulting in 2D HD dynamics and an inverse cascade of energy (Alexakis 2011). All of our simulations lie in the regime of strong background magnetic field, $V_A \gg 1$, making the rotation rate the main control parameter in our study. Does this asymptotic regime survive in the presence of rotation?

The relative strength of rotation is measured by the inverse Rossby number:

$$Ro^{-1} \equiv \frac{2\Omega L}{U}, \tag{2.6}$$

where L is a typical length-scale. This number measures the relative importance of the second term on the right hand side of equation (2.1) (the Coriolis force) to the advection term, which would determine whether or not the rotation affects the dynamics. Unlike the background magnetic field, the Coriolis force only directly affects the velocity fields. For regular hydrodynamics, in the absence of any magnetic field, strong Coriolis force,

$Ro^{-1} \gg 1$, acts to constrain the flow such that it doesn't vary along the z-direction, e.g. most of the energy lies in the $k_z = 0$ modes (Vallis 2017; Buzzicotti *et al.* 2018), which results in 2D HD on the x-y plane. If the fluid is ionized and initialized with a non-zero seed magnetic field, rapid rotation doesn't necessarily result in 2D HD dynamics because there is no direct constraint on the induced magnetic field. Instead, rapidly rotating dynamos are formed [CITE]. However, since our base state is the 2D HD regime in the y-z plane found when $V_A \gg 1$, rapid rotation is expected to act to constrain the flow and prevent it from varying in the z-direction. Note that, in this configuration, rotation is in the plane of the 2D dynamics, not out of the plane as is often the case when it itself is the cause of the bidimensionalization. Since rotation is now in the plane of the two-dimensional velocities, the Coriolis force is expected to deflect horizontal velocities out of the plane, as will be discussed in section 4 when we introduce a reduced model for this system following Montgomery & Turner (1981).

Our goal in this study is to investigate the effects that in-plane rotation has on the two-dimensional flow caused by a strong background magnetic field. In the next section we will describe results from direct numerical simulations of the RMHDB system for various rotation rates, paying particular attention to the resulting energy cascade and morphology of the flow field.

3. Strong background field limit: 3D RMHDB simulations

Equations (2.1)-(2.3) were solved numerically in a triply-periodic domain of side length 2π using the Geophysical High-Order Suite for Turbulence (GHOST) code (Mininni *et al.* 2011), with only slight modifications: the inclusion of a 'hyperviscosity' and a large-scale dissipation term called 'hypoviscosity'. The hyperviscosity replaces the regular viscous and magnetic diffusion terms with a Laplacian of a higher order, in our case $\nabla^2 \to -\nabla^4$. This higher order allows for the possibility of forcing at smaller length-scales while still properly resolving the smallest scales at moderate resolutions. As long as the order of the Laplacian is not very large, hyperviscosity has been shown to have no significant effect on the turbulent properties of 3D turbulence, and we expect the same to be the case for our work (Agrawal *et al.* 2020). The hypoviscosity, which would appear as $\nu_- \nabla^{-2}\boldsymbol{v}$ on the right hand side of equation (2.1) and as $\eta_- \nabla^{-2}\boldsymbol{b}$ on the right hand side of equation (2.2), acts as a large-scale dissipation term. Should an inverse cascade of a conserved quantity occur, this term ensures that no condensate forms, which would otherwise affect the cascades and inertial ranges (Alexakis & Biferale 2018). This is done by choosing the coefficients ν_- and η_- such that the kinetic and magnetic energy at the largest scales is smaller than that at subsequently smaller scales. The modified GHOST code which includes these alternative dissipative terms can be found in the Github repository of the first author (Benavides 2019). It is a standard parallel pseudo-spectral code with a fourth-order Runge–Kutta scheme for time integration and a two-thirds dealiasing rule. The three-dimensional forcing $\boldsymbol{f}$ was isotropic and constant in time, comprising of a summation of cosines with wavenumbers between $8 < |\boldsymbol{k}| < 10$ and random phases. The forcing wavenumber range was chosen in an attempt to properly resolve both an inverse cascade and a forward cascade. Its amplitude, f_0, was chosen so that $|\boldsymbol{v}| \sim 1$ in this forcing range. We do not force the induced magnetic field.

All runs, unless otherwise stated, were in the large background field regime with $V_A \approx 91$. We found this value to be large enough to produce the expected two-dimensionalization in the absence of rotation (Figure 1(a)). Larger background magnetic field values resulted in significant restrictions in the time-step which would limit our ability to perform the same parameter sweep. The Reynolds and magnetic Reynolds numbers, defined, respectively, as $Re \equiv L^3U/\nu$ and $Re_m \equiv L^3U/\eta$ when considering hyperviscous and hyperdiffusive terms as we do, measure the relative strength of the advection terms compared to the hyperviscous and magnetic hyperdiffusion terms. For the simulations we performed, the Reynolds and magnetic Reynolds numbers were large (approximately 300) and equal to each other, implying turbulent dynamics of both the velocity field as well as the induced magnetic field. We performed 14 runs at $V_A \approx 91$ but at different values of Ro^{-1}, ranging from $Ro^{-1} = 0$ to $Ro^{-1} = 29$. All averages and snapshots were taken at steady state. See Table 1 for details of the simulations and a description of how we measured the nondimensional numbers.

In this study, we are partly concerned with the behavior of the energy cascade as rotation is varied. We expect the presence of a bidirectional cascade, where a fraction of the energy input by the forcing goes to large scales and the rest goes to small scales. As such, we define a measure for the fraction of energy that goes to large scales in the form of kinetic energy, ε_-, and that which goes to small scales in the form of kinetic energy ε and magnetic energy ε_b. Since the large-scale magnetic energy dissipation is practically zero for every simulation performed, we ignore it from our analysis, as it plays no role. These measures are based on the dissipation rates from each of the three dissipation terms, and are defined in the following way:

$$\varepsilon_- \equiv \nu_-\langle\left|\nabla^{-1}\boldsymbol{v}\right|^2\rangle/I, \quad \varepsilon \equiv \nu\langle\left|\nabla^2\boldsymbol{v}\right|^2\rangle/I, \quad \varepsilon_b \equiv \mu\langle\left|\nabla^2\boldsymbol{b}\right|^2\rangle/I, \tag{3.1}$$

where $\langle\cdot\rangle$ represents a space- and time-average, and $I \equiv \langle \boldsymbol{f}\cdot\boldsymbol{v}\rangle$ is the space- and time-averaged energy injection rate. Energy balance at steady state tells us that $\varepsilon_- + \varepsilon + \varepsilon_b = 1$. In the limit of large Reynolds number and large forcing wavenumber, none of the energy injected is dissipated at the forcing scale and proper inertial ranges are formed. In this case, the dissipation rate at large scales represents the fraction of energy cascading to large scales, and similarly for the dissipation rate at small scales. Although our runs do not reach these idealized limits, the measures defined in equation (3.1) still accurately represent the presence of cascades, now with the caveat that a purely forward cascade might not show $\varepsilon_- = 0$ exactly. To complement these estimates for energy cascades, we will look at the spectral energy flux:

$$\Pi_{KE}(k) \equiv \left\langle \boldsymbol{v}^{<k}\cdot(\boldsymbol{v}\cdot\nabla\boldsymbol{v})\right\rangle, \tag{3.2}$$

$$\Pi_{ME}(k) \equiv -\left\langle \boldsymbol{v}^{<k}\cdot((\boldsymbol{B_0}+\boldsymbol{b})\cdot\nabla\boldsymbol{b})\right\rangle + \left\langle \boldsymbol{b}^{<k}\cdot(\boldsymbol{v}\cdot\nabla\boldsymbol{b}-(\boldsymbol{B_0}+\boldsymbol{b})\cdot\nabla\boldsymbol{v})\right\rangle, \tag{3.3}$$

where $\boldsymbol{v}^{<k}$ stands for a filtering of the velocity $\boldsymbol{v}$ in Fourier space so that only the wavenumbers with modulus smaller than k are kept. The flux $\Pi(k)$ expresses the rate at which energy is flowing out of scales larger than $\ell = 2\pi/k$ due to nonlinear interactions. Therefore, if energy is going from large to small scales, the energy flux will be positive, and *vice versa*. Finally, to quantify the amount and type of energy at each scale, we will also look at the energy spectra:

$$E_{KE}(k) \equiv \frac{1}{2}\sum_{|\boldsymbol{k}|=k}|\widehat{\boldsymbol{v}}|^2(\boldsymbol{k}), \quad E_{ME}(k) \equiv \frac{1}{2}\sum_{|\boldsymbol{k}|=k}|\widehat{\boldsymbol{b}}|^2(\boldsymbol{k}), \tag{3.4}$$

where $\widehat{\boldsymbol{v}}$ denotes the Fourier transform of $\boldsymbol{v}$.

Beginning from quasi-two-dimensional turbulence on the y-z plane at zero rotation, we found unexpected behavior with increasing rotation rate, resulting in the identification of four distinct regimes (Figure 1). Although not so apparent in the 3D simulations, these regimes are separated by seemingly sharp transitions, whose boundaries are determined in Section 4.

Regime I (Figure 1(a)), defined for runs with $Ro^{-1} < 0.65$, is characterized by the

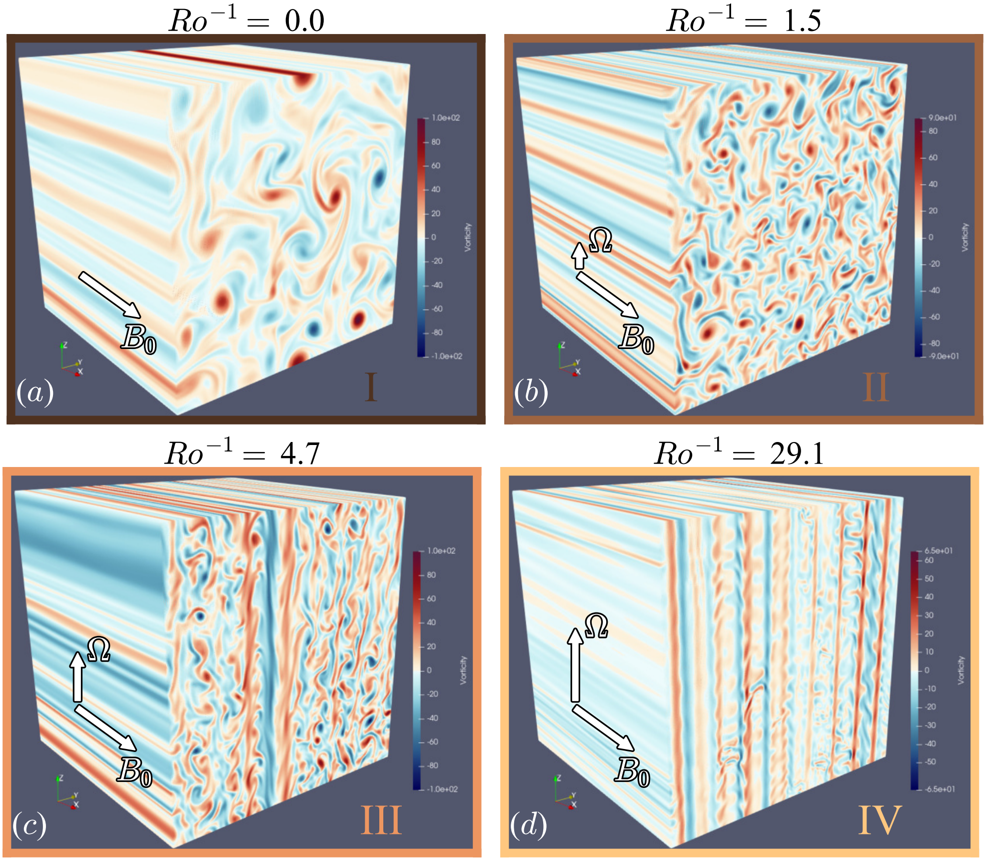

FIGURE 1. Snapshots of the field-aligned vorticity $\omega = \hat{x} \cdot (\nabla \times \boldsymbol{v})$, representing, from top left to bottom right, Regimes I (a), II (b), III (c), and IV (d), as rotation rate is increased. Regime I is characterized by an inverse or bidirectional cascade, Regime II with a purely forward cascade, Regime III with the formation of strong shear layers, and Regime IV with magnetically active shear layers. Regimes I-III have a negligible induced magnetic energy, unlike Regime IV whose magnetic energy dominates the dynamics (Figure 2).

presence of a bidirectional cascade. This can be seen in Figure 2 as a non-zero large-scale dissipation rate as well as in Figure 3(e), where the spectral energy transfers show that about half of the energy injected by the forcing goes to large scales (negative $\Pi(k)$) and the other half goes to small scales (positive $\Pi(k)$). The fraction of energy that goes to larger scales decreases with increasing rotation (Figure 2). At zero rotation we don't have a purely inverse cascade ($\varepsilon_- \approx 1$) due to a combination of finite background magnetic field strength and, as we will see in Section 4, the fact that we're forcing the out-of-plane velocity which acts as a passive scalar in the two-dimensionalized dynamics, thus contributing to a forward energy flux. If we were to force only the horizontal velocity components in the $k_x = 0$ wavenumber plane, we would expect to see $\varepsilon_- \approx 1$ at zero rotation. Figure 3(a) shows the kinetic and magnetic energy spectra, which demonstrates that the magnetic energy is orders of magnitude smaller than the kinetic energy (particularly at large scales) and that the largest scales have the most energy, providing further confirmation of the presence of an inverse cascade. The spike of magnetic energy at the forcing scale is due to the excitation of Alfvén waves from the isotropic forcing.

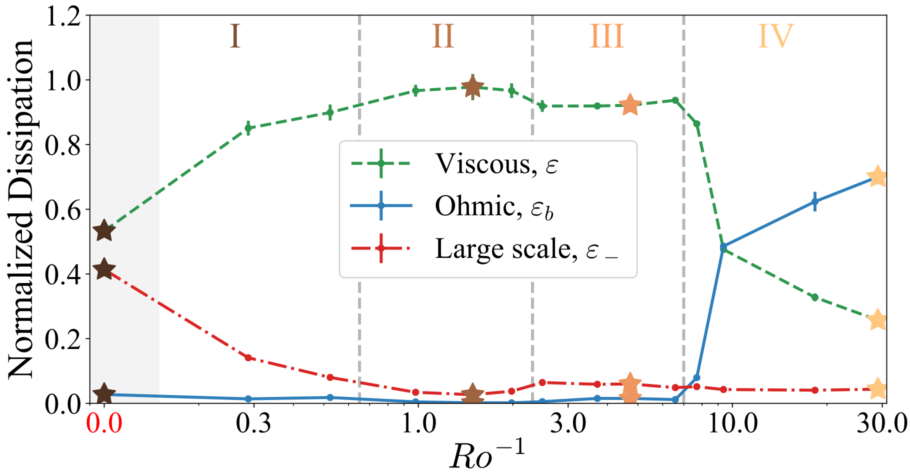

FIGURE 2. Dissipation rates normalized by the energy injection rate as a function of rotation rate measured by the inverse Rossby number Ro^{-1}. The blue solid line shows the Ohmic dissipation rate due to the magnetic diffusion term, ε_b, the green dashed line shows the viscous dissipation rate, ε, and the red dash-dotted line shows the large-scale dissipation rate due to the hypoviscosity, ε_-. Each regime is labelled at the top, and the vertical dashed lines represent boundaries between regimes, chosen based on the two-dimensional runs in Section 4. Stars represent runs whose snapshots are shown in Figure 1.

Regime II (Figure 1(b)), defined for runs with $0.65 < Ro^{-1} < 2.3$, is characterized by a purely forward cascade of energy (Figures 2 and 3(f)). This may come as a surprise, given that the dynamics are two-dimensional. The reason for this seemingly-contradictory state is that, while two-dimensional, all three velocity components are active in the dynamics and, furthermore, are coupled together with rotation. This results in a set of reduced two-dimensional, three-component (2D3C) equations which no longer conserve enstrophy, making a forward cascade of energy possible. The rotating 2D3C system will be discussed and explored numerically in Section 4.

Regime III (Figure 1(c)), defined for runs with $2.3 < Ro^{-1} < 7$, is characterized by the formation of strong shear-layers along the y-direction, consisting of uniform velocity in the x-z plane. The shear layers form when the rotational constraint on the dynamics at large scales becomes sufficiently large, requiring that $\partial_z \boldsymbol{v} \approx 0$ at those scales. The combination of $\partial_z = \partial_x = 0$ and incompressibility implies that $v_y = 0$ (since we're in a periodic domain), and thus that the last remaining component of the nonlinear advection term $v_y \partial_y = 0$ and nonlinearities are suppressed at large scales. Because of the suppressed nonlinearity at large scales, these shear layers form coherent structures that are fed directly by the forcing but that do not transfer that energy away, causing a build up of energy (not shown). The energy in the layers builds until a combination of the large-scale dissipation (Figure 2) and the nonlinear term (Figure 3(g)) are able to remove energy from those scales. Regimes I-III have negligible induced magnetic energy, as is observed in simulations of MHD with a strong background field (Alexakis 2011), and so the induced magnetic field plays an insignificant role in the dynamics.

This changes, however, in Regime IV (Figure 1(d)), defined for runs with $Ro^{-1} > 7$, where we have found the activation and growth of the induced magnetic field, which dominates both the energy as well as the nonlinear energy transfers (Figure 2). The nonlinear advection term in the momentum equation is suppressed for practically all

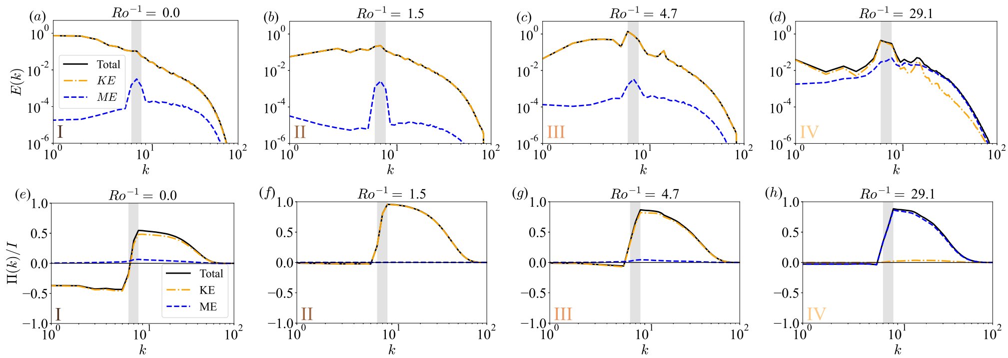

FIGURE 3. The time-averaged energy spectra (top row) and spectral energy flux (bottom row) for each Regime found in our simulations. The blue dashed line shows the magnetic components, either E_{ME} or Π_{ME}, the orange dash-dotted line shows the kinetic components, E_{KE} or Π_{KE}, and the solid black line shows their sum. The grey box represents the forcing range. These are from the same simulations shown in Figure 1 and which are starred in Figure 2.

System	B_0	V_A	Ω	k_f	f_0	Forcing type	ν	ν_-	Resolution	Count
(2.1)-(2.3)	40	91	[0 − 50]	8-10	9	Constant Amplitude	2e-6	0.2	256^3	14
(2.1)-(2.3)	20	47	[0 − 22]	8-10	9	Constant Amplitude	2e-6	0.2	256^3	11
(2.1)-(2.3)	10	25	[0 − 22]	8-10	9	Constant Amplitude	2e-6	0.2	256^3	5
(4.1)-(4.2)	∞	∞	[0 − 20]	12	1.0	Random	4e-7	1.0	512^2	23

TABLE 1. A summary of the runs performed for this work. All runs have hyper- and hypo-viscosity of the same order (Section 3). For runs with a magnetic field, $\mu = \nu$ and $\mu_- = \nu_-$. The simulations used Alfvénic units so that $B_0/\sqrt{\rho_0\mu_0} \to B_0$ and the other ρ_0 was absorbed into the pressure. k_f is the forcing wavenumber, f_0 is the forcing amplitude (for constant amplitude forcing) or energy injection rate (for the random forcing). The typical velocity, U, was calculated for each run using the four-fifths law $U^3 = (4/5)Ik_f^{-1}$, where $I \equiv \langle \boldsymbol{f} \cdot \boldsymbol{v} \rangle$ is the time- and space-averaged energy injection rate, and k_f is the forcing wavenumber. The typical length-scale was chosen to be $L = k_f^{-1}$ in estimates of dimensionless numbers. The count is the number of runs in that set.

scales (Figure 3(h)), leading to laminar-like shear-layer structures (Figure 1(d)) and a magnetic field which moves the energy around.

We expect the boundaries between Regimes I-III to be independent of V_A, as they are part of the asymptotic 2D3C HD dynamics whose sole parameter is the rotation rate. We confirm this in the next section, which deals specifically with this asymptotic set of equations, by showing that the regime transitions happen for the same values of Ro^{-1}. The transition from Regime III to IV is of a different nature and represents a breakdown of the hydrodynamic behavior found for lower rotation rates. This transition is found to be V_A-dependent, and will be discussed briefly in Section 5.

4. Comparison to rotating two-dimensional, three-component model

Regimes I-III can be better understood by considering the asymptotic limit of equations (2.1) - (2.3) when taking $V_A \to \infty$ and keeping $Ro^{-1} \sim \mathcal{O}(1)$. The procedure is almost identical to that done in Montgomery & Turner (1981), with the exception that we include the Coriolis term, and so we only briefly discuss it here. The process results in a set of three dynamical equations and one nonlinear constraint for the three variables: $\psi(y, z, t)$

the streamfunction for the in-plane velocities, $v_x(y,z,t)$ the out-of-plane velocity, and $A(y,z,t)$ the potential for the in-plane magnetic field. In the case of no rotation the nonlinear constraint, $[A, v_x] \equiv \partial_y A \partial_z v_x - \partial_y v_x \partial_z A = 0$, is thought to be satisfied because both A and v_x follow the same advection equation. However, in the case of nonzero rotation, the equation for v_x has the Coriolis force which is not present in the induction equation for A. This results in the novel constraint that either $A' \equiv \delta A/\delta v_x = 0$ or $v_y = \partial_z \psi = 0$, where A' is the functional derivative of A with respect to v_x. Our three-dimensional simulations from Section 3 seem to be consistent with these constraints, where, for $Ro^{-1} < 7$, we have $A \approx 0$ but $v_y \neq 0$ and, for $Ro^{-1} > 7$, we have $A \neq 0$ but $v_y = \partial_z \psi \approx 0$. Simulating the full three equations plus nonlinear constraint is too difficult, but one can set, by hand, how the nonlinear constraint is satisfied. We decided to assume $A = 0$ and study the reduced dynamics in Regimes I-III, knowing that it would not capture the transition to Regime IV. The resulting equations form the two-dimensional, three-component (2D3C) system with in-plane rotation:

$$\frac{\partial v_x}{\partial t} + [v_x, \psi] = 2\Omega \frac{\partial \psi}{\partial z} + \nu \nabla_\perp^2 v_x + f_x, \tag{4.1}$$

$$\frac{\partial \omega}{\partial t} + [\omega, \psi] = 2\Omega \frac{\partial v_x}{\partial z} + \nu \nabla_\perp^2 \omega + f_\omega, \tag{4.2}$$

where $\nabla_\perp = (0, \partial_y, \partial_z)$, $\omega = \hat{x} \cdot (\nabla \times \boldsymbol{v}) = -\nabla_\perp^2 \psi$ is the out-of-plane vorticity of the in-plane velocities, $\perp$ implies the directions perpendicular to the background magnetic field, and $f_\omega = \hat{x} \cdot (\nabla_\perp \times \boldsymbol{f}_\perp)$.

The Coriolis force now couples the two equations together, making what would otherwise be a passive tracer into an active one. In fact, for non-zero rotation, it can be shown that the 2D3C rotating system conserves kinetic energy and helicity:

$$KE = \frac{1}{2} \int v_x^2 + |\nabla \psi|^2 \; d^2x, \tag{4.3}$$

$$H = \int v_x \omega \; d^2x. \tag{4.4}$$

These are the same conserved quantities as in 3D HD, but we emphasize that the dynamics are two-dimensional and are occurring on the y-z plane. This is in contrast to the case of zero rotation, where the system conserves (separately) the in-plane kinetic energy $\int |\nabla \psi|^2 \; d^2x$ and the out-of-plane kinetic energy $\int v_x^2 \; d^2x$, as well as the enstrophy, $\int \omega^2 \; d^2x$. The conservation of enstrophy can be shown to prevent the existence of a forward cascade of in-plane kinetic energy (Alexakis & Biferale 2018). Without the restriction of enstrophy conservation, though, the kinetic energy may go downscale in a forward cascade, even if one doesn't force the out-of-plane component.

Equations (4.1) and (4.2), with modified hyper- and hypo-viscosities as in the 3D simulations, were solved numerically in a doubly-periodic domain of side length 2π using the 2D predecessor of GHOST. The code can be found in the Github repository of the first author (Benavides 2020). Unlike the 3D runs, whose forcing function had a constant amplitude in time, the 2D3C runs had random (white-in-time) forcing. At each time step, a wavenumber $\boldsymbol{k}_r$ of magnitude k_f was chosen at random, and $\hat{f}_\omega(\boldsymbol{k})$ (Fourier transform of f_ω) was set to zero everywhere except for at $\boldsymbol{k}_r$, where it had a magnitude $k_f\sqrt{2f_0/\Delta t}$ (Chan *et al.* 2012). This has the effect of setting the energy injection rate for the in-plane flow to be $I = \langle \psi f_\omega \rangle = f_0$ on average. The same forcing was applied for f_x, but with an amplitude of $\sqrt{2f_0/\Delta t}$ instead, giving the same results. Therefore, half of the energy was injected into the in-plane flow and the other half in the out-of-plane velocity. For all of the runs reported, $f_0 = 1$ and $k_f = 12$. See Table 1 for details on the runs.

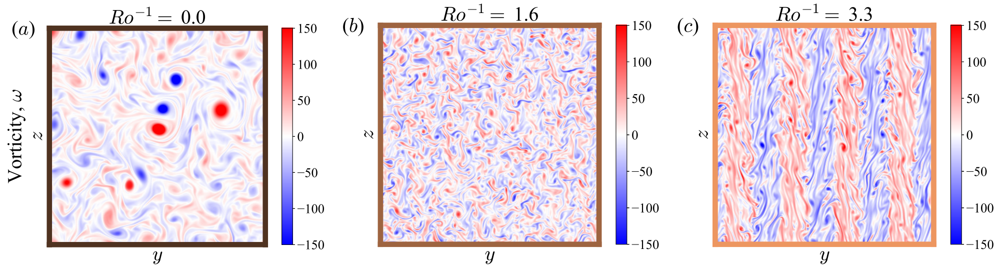

FIGURE 4. Snapshots of the out-of-plane vorticity, $\omega = \hat{x}\cdot(\nabla\times\boldsymbol{v}) = -\nabla_\perp^2\psi$, for the 2D3C rotating simulations, representing, from left to right, Regimes I (a), II (b), and III (c), as rotation is increased. We see striking similarities to Figure 1, confirming that the asymptotic 2D3C model captures the different regimes found in the 3D simulations of Section 3.

The goal of these simulations was to reproduce the parameter sweep performed in Section 3, but with the added advantage of working with a two-dimensional code, thus allowing a larger quantity of runs, higher resolutions (larger Reynolds numbers, around 590), and longer time integration. We performed 23 runs, with Ro^{-1} ranging from 0 to about 5, at four times the horizontal resolution. Our results confirm the presence of Regimes I-III, going from a bidirectional cascade to a forward cascade to a shear-layer configuration (Figure 4).

At zero rotation we see a bidirectional cascade with half of the injected energy going to large scales and half going to small scales (Figure 5), similar to what was found in the 3D runs (Figure 2). For the 2D3C rotating system we understand that this is the case because of the choice of forcing, which, as we mentioned, injects half of the energy to the in-plane flow and the other half to the out-of-plane velocity. Since the two flows are completely decoupled at zero rotation, they each follow the standard behavior observed in 2D and passive tracer turbulence, that is, an inverse and forward cascade of energy, respectively. As we increase rotation, the Coriolis force couples the two fields, enstrophy is no longer conserved, and the in-plane velocities no longer cascade all the injected energy to large scales, resulting in a bidirectional cascade with decreasing inverse energy flux. There seems to be an approximately linear approach to zero inverse energy flux, and at $Ro^{-1} \approx 0.65$ there is a transition to a purely forward cascade. With a larger number of simulations, Regimes I and II are much more clearly separated, and their transitions appear to be sharp (Figure 5). This transition is qualitatively similar to other bidirectional to forward cascade transitions seen in other studies and could hint at a universal mechanism responsible for this transition (Seshasayanan *et al.* 2014; Seshasayanan & Alexakis 2016; Benavides & Alexakis 2017; van Kan & Alexakis 2020).

Upon further increase of the rotation, the forward cascade regime (Regime II) transitions to a shear layer configuration (Figure 4(c)), entering Regime III. This corresponds to the case when the Coriolis force dominates at large scales, making the dominant balance in equations (4.1) and (4.2) $\partial_z\psi \approx \partial_z v_x \approx 0$, hence the layers. There are a few differences in the morphology of the shear layers seen for these runs, compared to Regime III in the 3D simulations (Figure 1(c)). Here they take up the whole domain and also appear to equilibrate at scales larger than the forcing, through a series of mergers (not shown). Neither of these characteristics are seen in the shear layers of the 3D simulations. We believe this might be due to a few factors, including the longer integration times and the change in forcing. A surprising feature of this transition, revealed by the better-resolved parameter sweep, is that it looks to be discontinuous (Figure 5) †. Discontinuities

† An increase in large-scale dissipation marks this transition *not* because an inverse cascade

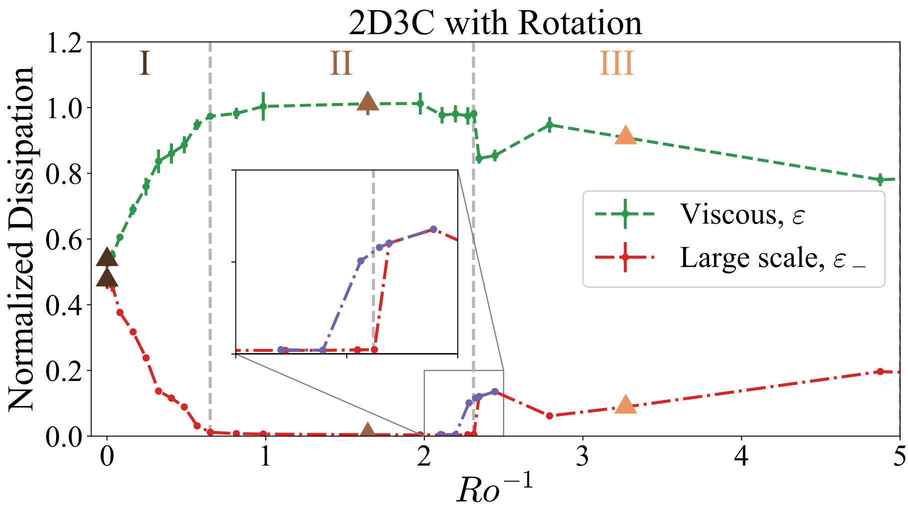

FIGURE 5. Dissipation rates normalized by the energy injection rate as a function of rotation rate measured by the inverse Rossby number Ro^{-1}. The green dashed line shows the viscous dissipation rate, ε, the red dash-dotted line shows the large-scale dissipation rate due to the hypoviscosity, ε_-, and the purple dash-dotted line shows the same but for hysteresis runs initialized with layers. Each regime is labelled at the top, and the vertical dashed lines represent boundaries between regimes. These denoted boundaries are placed at the same value of Ro^{-1} as those seen in Figure 2. Triangles represent runs whose snapshots are shown in Figure 4.

are a characteristic of subcritical bifurcations, which should also display hysteresis. By initializing in the layered regime, we confirmed the presence of hysteresis as we reduced the rotation rate (Figure 5 inset).

Despite differences in the forcing, Reynolds numbers, and values of V_A, the regime transitions seem to occur for the same values of Ro^{-1}, suggesting that the rotating 2D3C system successfully describes the dynamics observed in the 3D simulations from Section 3 and that Regimes I-III are robust properties of the system. The two-dimensional asymptotic system has allowed us to perform a more detailed parameter sweep of this parameter space, and has revealed sharp transitions and nontrivial behavior near those transitions which we did not anticipate from the 3D simulations.

5. Discussion & Conclusions

We've investigated the turbulent dynamics of rotating magnetohydrodynamics in the presence of a strong uniform background magnetic field which is misaligned with the rotation axis. Our investigations have revealed surprising behavior, confirmed both by three-dimensional and a two-dimensional three-component asymptotic model, as rotation rate is increased. We observed the weakening of the inverse cascade, a transition to a purely forward cascade for relatively weak rotation, and eventually the formation a shear-layer regime at larger rotation rates. The strong sensitivity of the inverse cascade to

forms (a weakness of this measure), but because of a lack of separation of scales. The layers form at or near the forcing scale and remain there as coherent structures, fed directly by the forcing, resulting in a build up of energy at those scales. This, in turn, results in a larger dissipation rate from the large-scale dissipation. If we were to perform runs at a larger k_f, this effect would disappear. The discontinuous transition is also observed in the kinetic energy, which is not shown.

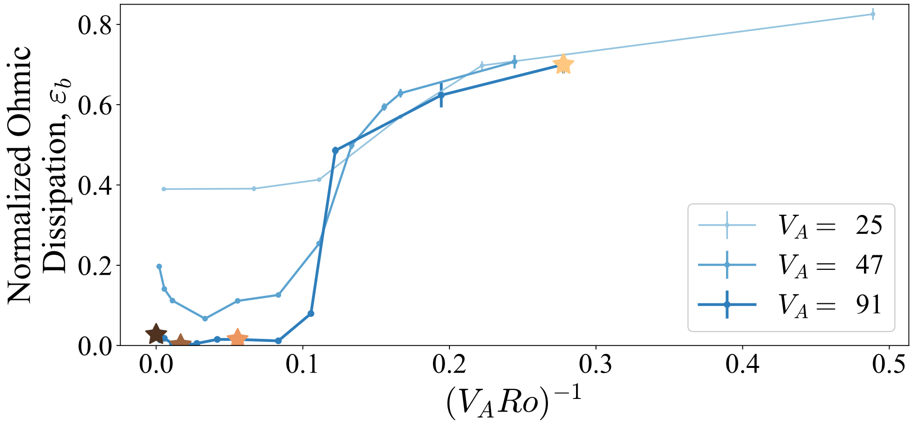

FIGURE 6. Normalized Ohmic dissipation, ε_b, versus $(V_A Ro)^{-1}$. The Ohmic dissipation represents a measure of how active the induced magnetic field is in the dynamics. We see that, for three values of V_A, the induced magnetic field begins to dominate the dynamics once $(V_A Ro)^{-1} > 0.1$, in other words when $Ro^{-1} > 0.1V_A$. $V_A Ro$ is also referred to as the Lehnert number (Lehnert 1955). Stars represent runs whose snapshots are shown in Figure 1.

in-plane rotation could have significant implications for the morphology of astrophysical flows, which often have both rotation and a background magnetic field. Even for relatively weak rotation ($Ro^{-1} \sim 1$) the inverse cascade is entirely suppressed. Seeing as an inverse cascade is considered to be necessary for the formation of jets on gas giant planets, this phenomenon could be a tentative alternative explanation for the weakening of the jets in the depths of their atmospheres, as seen by the *Juno* mission on Jupiter (Kaspi *et al.* 2018). In the outer electrically-neutral regions the jets can form because of the rapid rotation. These rotation-aligned jets would penetrate deep into the interior, were it not for the ionization that occurs at depth, leading to low Re_m MHD dynamics which is assumed to suppress the jets via Ohmic dissipation (Liu *et al.* 2008). Our work reveals another potential alternative, where a misalignment of the rotation and background field cause the localized turbulent dynamics to cascade energy forward instead of inversely, thereby taking away the dynamical origin of the jets. Apart from the astrophysical implications, the rotating 2D3C model might be of interest to those studying phase transitions in turbulence (Alexakis & Biferale 2018) – particularly those interested in the transition from a forward to a bidirectional cascade, since, as far as we are aware, this model is the only two-dimensional hydrodynamical one with this behavior.

At the largest rotation rotates, our 3D simulations showed a sudden activation of the induced magnetic field, signaling the breakdown of the assumption that $A = 0$ for the asymptotic model. The flow remained two-dimensional, but the dynamics became significantly different from the hydrodynamic shear-layer regime and were almost entirely in the induced magnetic field. We do not know the physical origin of this transition, or why it also seems to be sharp, but a series of simulations at lower V_A values (Table 1) reveal that the transition happens when $V_A \sim Ro^{-1}$, which represents roughly the point at which the inertial wave frequency begins to dominate over the Alfvén wave frequency (Figure 6). Interestingly, this transition seems to sharpen towards a critical value as the background magnetic field strength increases. This has the important implication that, when considering the limit of strong rotation and strong background magnetic field, the order in which those limits are taken matters. If $Ro^{-1} < 0.1V_A$, then one would expect a hydrodynamical regime, whereas if $Ro^{-1} > 0.1V_A$ a magnetically-dominated regime is expected.

Acknowledgments

This research was carried out in part during the 2019 Summer School at the Center for Computational Astrophysics, Flatiron Institute. The Flatiron Institute is supported by the Simons Foundation. SJB acknowledges funding from a grant from the National Science Foundation (OCE-1459702) and from the National Aeronautics and Space Administration (Proposal Number: PLANET20-0021) issued through the Future Investigators in NASA Earth and Space Science and Technology (NNH19ZDA001N-FINESST) within the NASA Research Announcement (NRA): Research Opportunities in Space and Earth Sciences (ROSES-2019).

Declaration of Interests

The authors report no conflict of interest.

REFERENCES

Agrawal, Rahul, Alexakis, Alexandros, Brachet, Marc E. & Tuckerman, Laurette S. 2020 Turbulent cascade, bottleneck, and thermalized spectrum in hyperviscous flows. *Phys. Rev. Fluids* **5**, 024601.

Alexakis, Alexandros 2011 Two-dimensional behavior of three-dimensional magnetohydrodynamic flow with a strong guiding field. *Phys. Rev. E* **84**, 056330.

Alexakis, A. & Biferale, L. 2018 Cascades and transitions in turbulent flows. *Physics Reports* **767-769**, 1 – 101.

Baklouti, F. S., Khlifi, A., Salhi, A., Godeferd, F., Cambon, C. & Lehner, T. 2019 Kinetic-magnetic energy exchanges in rotating magnetohydrodynamic turbulence. *Journal of Turbulence* **20** (4), 263–284.

Bell, N K & Nazarenko, S V 2019 Rotating magnetohydrodynamic turbulence. *Journal of Physics A: Mathematical and Theoretical* **52** (44), 445501.

Benavides, Santiago J. 2019 Geophysical high-order suite for turbulence. *GitHub repository* **https://github.com/s-benavides/GHOST/tree/pre-release-2**, Commit: 2caaa43aad8b9378ec154bfbc26e4c85d947a4cc.

Benavides, Santiago J. 2020 Rot2d3c. *GitHub repository* **https://github.com/s-benavides/Rot2D3C**, Commit: 2d511888b78c451fc7b26352916a6ff40ee98b93.

Benavides, Santiago Jose & Alexakis, Alexandros 2017 Critical transitions in thin layer turbulence. *Journal of Fluid Mechanics* **822**, 364–385.

Benavides, Santiago J. & Flierl, Glenn R. 2020 Two-dimensional partially ionized magnetohydrodynamic turbulence. *Journal of Fluid Mechanics* **900**, A28.

Boffetta, Guido & Ecke, Robert E. 2012 Two-dimensional turbulence. *Annual Review of Fluid Mechanics* **44** (1), 427–451, arXiv: https://doi.org/10.1146/annurev-fluid-120710-101240.

Buzzicotti, Michele, Aluie, Hussein, Biferale, Luca & Linkmann, Moritz 2018 Energy transfer in turbulence under rotation. *Phys. Rev. Fluids* **3**, 034802.

Chan, Chi-kwan, Mitra, Dhrubaditya & Brandenburg, Axel 2012 Dynamics of saturated energy condensation in two-dimensional turbulence. *Phys. Rev. E* **85**, 036315.

Diamond, P H, Itoh, S-I, Itoh, K & Hahm, T S 2005 Zonal flows in plasma—a review. *Plasma Physics and Controlled Fusion* **47** (5), R35–R161.

Favier, B. F.N., Godeferd, F. S. & Cambon, C. 2012 On the effect of rotation on magnetohydrodynamic turbulence at high magnetic Reynolds number. *Geophysical and Astrophysical Fluid Dynamics* **106** (1), 89–111, arXiv: 1103.6236.

Frisch, U. 1995 *Turbulence: the legacy of AN Kolmogorov*. Cambridge University Press.

Galtier, Sébastien 2014 Weak turbulence theory for rotating magnetohydrodynamics and planetary flows. *Journal of Fluid Mechanics* **757** (6), 114–154.

van Kan, Adrian & Alexakis, Alexandros 2020 Critical transition in fast-rotating turbulence within highly elongated domains. *Journal of Fluid Mechanics* **899**, A33.

Kaspi, Y., Galanti, E., Hubbard, W. B., Stevenson, D. J., Bolton, S. J., Iess, L., Guillot, T., Bloxham, J., Connerney, J. E. P., Cao, H., Durante, D., Folkner, W. M., Helled, R., Ingersoll, A. P., Levin, S. M., Lunine, J. I., Miguel, Y., Militzer, B., Parisi, M. & Wahl, S. M. 2018 Jupiter's atmospheric jet streams extend thousands of kilometres deep. *Nature* **555**, 223 EP –.

Lehnert, B. 1955 The decay of magneto-turbulence in the presence of a magnetic field and coriolis force. *Quarterly of Applied Mathematics* **12** (4), 321–341.

Liu, Junjun, Goldreich, Peter M. & Stevenson, David J. 2008 Constraints on deep-seated zonal winds inside Jupiter and Saturn. *Icarus* **196** (2), 653–664.

Menu, Mélissa D., Galtier, Sébastien & Petitdemange, Ludovic 2019 Inverse cascade of hybrid helicity in $b\Omega$-mhd turbulence. *Phys. Rev. Fluids* **4**, 073701.

Mininni, Pablo D., Rosenberg, Duane, Reddy, Raghu & Pouquet, Annick 2011 A hybrid mpi–openmp scheme for scalable parallel pseudospectral computations for fluid turbulence. *Parallel Computing* **37** (6), 316 – 326.

Montgomery, David & Turner, Leaf 1981 Anisotropic magnetohydrodynamic turbulence in a strong external magnetic field. *Physics of Fluids* **24** (5), 825–831.

Pouquet, A., Rosenberg, D., Stawarz, J.E. & Marino, R. 2019 Helicity dynamics, inverse, and bidirectional cascades in fluid and magnetohydrodynamic turbulence: A brief review. *Earth and Space Science* **6** (3), 351–369, arXiv: https://agupubs.onlinelibrary.wiley.com/doi/pdf/10.1029/2018EA000432.

Rhines, Peter B. 1975 Waves and turbulence on a beta-plane. *Journal of Fluid Mechanics* **69** (3), 417–443.

Seshasayanan, Kannabiran & Alexakis, Alexandros 2016 Critical behavior in the inverse to forward energy transition in two-dimensional magnetohydrodynamic flow. *Physical Review E* **93** (1), 1–13.

Seshasayanan, Kannabiran, Benavides, Santiago Jose & Alexakis, Alexandros 2014 On the edge of an inverse cascade. *Physical Review E - Statistical, Nonlinear, and Soft Matter Physics* **90** (5), 1–5.

Shebalin, John V. 2006 Ideal homogeneous magnetohydrodynamic turbulence in the presence of rotation and a mean magnetic field. *Journal of Plasma Physics* **72** (4), 507–524.

Tobias, Steven M, Diamond, Patrick H & Hughes, David W 2007 β-plane magnetohydrodynamic turbulence in the Solar Tachocline. *The Astrophysical Journal* **667**, 113–116.

Vallis, Geoffrey K 2017 *Atmospheric and oceanic fluid dynamics*. Cambridge University Press.